Comparison of a grid-based CFD method and vortex dynamics predictions of low Reynolds number cylinder flows

L. Baranyi
Department of Fluid and Heat Engineering
University of Miskolc, Hungary

R. I. Lewis
University of Newcastle upon Tyne
UK

ABSTRACT

Computational fluid dynamics models range from the finite difference type grid-based method to the Lagrangian style vortex cloud simulation technique for solving the Navier-Stokes equations. This paper undertakes a comparison of these two methods for the classical datum bluff body case of flow past a stationary circular cylinder at low Reynolds numbers in the range 10 to 220. Comparisons include time-history, time-mean and root-mean-square values of oscillating drag and lift coefficients, frequency of vortex shedding and related vortex street wake flow patterns. Particularly close agreement was obtained for Strouhal number versus Reynolds number, and good agreement for time-mean value of drag coefficients; comparison was also made with experimental results. Attempts are also made to calculate the skin friction and surface pressure components of the cylinder drag, revealing the significance of skin friction drag within this range and its relative insignificance above a Reynolds number of 220.

NOMENCLATURE

C_D	drag coefficient
C_{Df}	drag coefficient due to skin friction
C_L	lift coefficient
C_{pb}	base pressure coefficient
d	cylinder diameter, length scale
D	dilation, drag force
f_v	vortex shedding frequency
$k(s_m,s_n)$, $K(s_m,s_n)$	coupling coefficients linking points m and n on a body
L	lift force
p	pressure, non-dimensionalised by ρU^2
Re	Reynolds number, Ud/ν
St	Strouhal number, $f_v d/U$
t	time, nondimensionalised by d/U
u,v	velocities in x,y direction, (for grid-based method, nondimensionalised by U)
U	free stream velocity, velocity scale
U_∞, V_∞	velocity components of W_∞ in the x,y directions
U_{mj}, V_{mj}	velocity components at m due to a unit strength vortex element at j
v_{sn}	body surface velocity at point n
W_∞	uniform stream at angle of incidence α_∞
x,y	Cartesian co-ordinates, (for grid-based method, nondimensionalized by d)
α_∞	incidence angle of uniform stream W_∞
β_m	body profile slope at point m
γ	surface sheet vorticity strength
$\Delta\Gamma_j$	discrete vortex element strength
Δt	discrete time step (nondimensionalised by d/U)
μ	viscosity
ρ	fluid density
ν	kinematic viscosity
ω	vorticity

Paper No. 2983. Manuscript received 3 May 2005, revised version received 31 August 2005, accepted 26 September 2005.

Subscripts

c	critical
D	drag
f	skin friction
L	lift
m, *n*	points on a body surface (vortex cloud modelling)
mean	time-mean value
n	normal
pb	base pressure
pot	potential flow
rms	root-mean-square value

1.0 INTRODUCTION

An interest in the formation of vortex streets behind bluff bodies has fascinated large numbers of researchers since the early experiments of Strouhal[1] in 1878 concerning the generation of 'Aeolean tones' and the famous 1911 paper by Theodore von Kármán[2] bequeathing his name to the 'von Kármán vortex street'. Serious early attempts at discrete vortex modelling were made by Rosenhead[3] (1931), who studied the related phenomenon of the Kelvin-Helmholtz instability of vortex sheets. Abernathy and Kronauer[4] (1962) extended Rosenhead's model to simulate the instabilities of a parallel pair of vortex sheets of equal and opposite strength subjected to an initial sinusoidal perturbation along their length in various combinations akin to two separating vortex sheets released by a bluff body. Also asserted by these authors was the constancy of mean drag coefficient and Strouhal number for a circular cylinder over a wide range of Reynolds numbers, e.g. Re = 300 to 100,000, demonstrating the negligible influence of viscosity upon these flows. Below Re ≈ 300 viscosity is very important, while above this range three-dimensional instabilities occur which disturb the regularity of the von Kármán vortex wake. Within this range however there are considerable variations of both Strouhal number and cylinder drag coefficients, which are one interest of the present study.

A huge number of researchers have investigated flow around a single circular cylinder through experimental, theoretical, and numerical approaches. Despite its simple geometry, the problem is not only extremely complex but also one with many applications. Knowledge of flow patterns around bluff bodies is important in the design of large structures such as smokestacks or bridges, which in winds are often subjected to large amplitude oscillation due to alternating vortex shedding, sometimes causing collapse of the structure. Slender struts or tubes are likewise subject to vibration due to vortex shedding, which can also cause noise generation in both external aerodynamics and internal aerodynamic applications such as turbomachinery or heat exchangers.

This problem is of such practical importance that there are numerous studies dealing with flow past cylinders that are fixed, oscillating, rotating, or in orbital motion. Among these, the fixed cylinder is usually the starting point of investigations, as it is relatively simple to carry out experiments on, and thus also for numerical studies, it is favoured because comparison with experimental data is possible to confirm validity of the computer method used. Roshko[7], Norberg[8], and Bearman[9] are among those who have provided invaluable experimental data on flow around a fixed cylinder. Computations on the same problem have been performed by many researchers, including Kawamura and Kuwahara[10], Braza *et al*[11] and Karniadakis and Triantafyllou[12].

The main purpose of this study is to compare two very different CFD methods against the important datum case of flow past a stationary circular cylinder at low Reynolds numbers. The first author has developed a finite difference method based on Eulerian description with grid transformation that facilitates simulation of the flow of a viscous fluid past a cylinder. This was developed to study the flow past an oscillating cylinder or past a cylinder in orbital motion, Baranyi[5], and his method is reviewed briefly in Section 2.1 for application to a stationary cylinder. The second author on the other hand has developed a vortex cloud analysis that follows the creation and diffusion from the body surface in Lagrangian fashion, Lewis[6], and that is well suited for modelling separated flows where boundary layer modelling is less key. This analysis is reviewed briefly in Section 2.2. Both methods deliver solutions of the Navier-Stokes equations for two-dimensional flow and are thus suited to simulation of cylinder wake studies in the low Reynolds number range 10 to 220.

2.0 OVERVIEW OF THE TWO METHODS OF ANALYSIS

This section gives an overview of the grid-based and vortex cloud methods for simulating a low Reynolds number flow around a circular cylinder placed in a uniform stream.

2.1 Overview of the grid-based method of CFD analysis

The first author's earlier studies dealt with computation of the flow around a fixed circular cylinder at different Reynolds numbers, from Re = 10 to 1000, and up to Re = 180 for an oscillating cylinder, e.g. Baranyi and Shirakashi[13], and good agreement was obtained with experimental data for the variation of Strouhal number and time-mean drag coefficient with Reynolds number, especially up to Re = 190 above which three-dimensional instabilities occur. Further features of flow are investigated for a fixed cylinder in Baranyi[14] and the time-mean value of base pressure coefficient, which influences the near-wake structure, compares well with the experimental data of Roshko[15]. In Baranyi[14] the energy equation for a stationary circular cylinder with constant surface temperature placed in a uniform flow is also solved from Re = 50 to 180 and the predicted dimensionless heat transfer coefficient or Nusselt number agrees well with available experimental results. In Baranyi and Lakatos[16] computational results obtained by this method are compared in the Reynolds number domain of Re = 50 – 180 with existing experimental results for the root-mean-square value of lift coefficients shown in Norberg[17] and a very good agreement is observed. Additional evidence for the reliability of the method has been given by comparison with other computational methods. De Sampaio[18] reports that his results for time-mean drag coefficient, obtained by the finite element method, agree well with those in Baranyi[14].

At the time Baranyi and Shirakashi[13] was published the computing power of computers were somewhat limited. In this paper some of the earlier computations are repeated with much finer temporal and spatial resolution, and new computations have also been added and compared with those of the vortex cloud method.

2.1.1 Governing equations

Constant property incompressible Newtonian fluid flow is assumed. when deriving the governing equations, which in non-dimensional forms are the Navier-Stokes equations, the equation of continuity and a Poisson equation for pressure:

$$\frac{\partial u}{\partial t}+u\frac{\partial u}{\partial x}+v\frac{\partial u}{\partial y}=-\frac{\partial p}{\partial x}+\frac{1}{\mathrm{Re}}\left(\frac{\partial^2 u}{\partial x^2}+\frac{\partial^2 u}{\partial y^2}\right); \quad \ldots (1)$$

$$\frac{\partial v}{\partial t}+u\frac{\partial v}{\partial x}+v\frac{\partial v}{\partial y}=-\frac{\partial p}{\partial y}+\frac{1}{\mathrm{Re}}\left(\frac{\partial^2 v}{\partial x^2}+\frac{\partial^2 v}{\partial y^2}\right); \quad \ldots (2)$$

$$D=\frac{\partial u}{\partial x}+\frac{\partial v}{\partial y}=0; \quad \ldots (3)$$

$$\nabla^2 p=\frac{\partial^2 p}{\partial x^2}+\frac{\partial^2 p}{\partial y^2}=2\left[\frac{\partial u}{\partial x}\frac{\partial v}{\partial y}-\frac{\partial u}{\partial y}\frac{\partial v}{\partial x}\right]-\frac{\partial D}{\partial t} \quad \ldots (4)$$

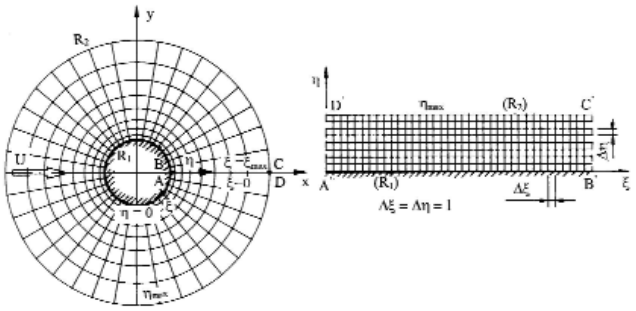

Figure 1. Physical and computational planes.

The gravity force is included in the pressure terms in Equations (1) and (2). Although the dilation D is theoretically zero by continuity (3), it is advisable to retain the term $\partial D/\partial t$ to avoid computational instability.

Boundary conditions:
(R_1) cylinder surface: $u = v = 0$;

$$\frac{\partial p}{\partial n} = \frac{1}{\mathrm{Re}}\nabla^2 v_n;$$

(R_2) undisturbed domain: $u = u_{pot}$; $v = v_{pot}$

$$\frac{\partial \mathrm{p}}{\partial \mathrm{n}} = \left(\frac{\partial \mathrm{p}}{\partial \mathrm{n}}\right)_{pot}$$

Here subscript *pot* stands for potential flow, and n denotes the outer normal along the cylinder surface.

2.1.2 Transformation of domain and equations and applied numerical methods

To avoid interpolation leading to poor solutions, a boundary-fitted coordinate system is used, allowing boundary conditions to be imposed accurately. By using unique, single-valued functions, the physical domain (x, y, t) can be mapped into a computational domain (ξ,η,τ)

$$\begin{aligned} x(\xi,\eta) &= R(\eta)\mathrm{Cos}\left[g(\xi)\right] \\ y(\xi,\eta) &= -R(\eta)\mathrm{Sin}\left[g(\xi)\right] \end{aligned} \qquad \ldots (5)$$

$t = \tau$
where the dimensionless radius is given by

$$R(\eta) = R_1 \exp\left[f(\eta)\right] \qquad \ldots (6)$$

This choice of the structure of the mapping functions automatically assures that the obtained grid is orthogonal on the physical plane for arbitrary functions $f(\eta)$ and $g(\xi)$. In this study the following linear mapping functions are used:

$$g(\xi) = 2\pi\frac{\xi}{\xi_{max}}; \quad f(\eta) = \frac{\eta}{\eta_{max}}\mathrm{Log}\left(\frac{R_2}{R_1}\right) \qquad \ldots (7)$$

where subscript *max* refers to maximum value.

Using mapping functions (7) cylindrical coordinates with logarithmically spaced radial cells are obtained on the physical plane, providing a fine grid scale near the cylinder wall and a coarse grid in the far field. Using Equations (5) – (7), the governing Equations (1) – (4) and boundary conditions can be transformed, although space does not permit these to be shown here.

The transformed governing equations are solved by using the finite difference method. Space derivatives are approximated by fourth order central difference formulae, except for the convective terms for which a third order modified upwind scheme is used[10]. The Poisson equation for pressure is solved by the successive over-relaxation (SOR) method. The Navier-Stokes equations are integrated explicitly and the continuity equation is satisfied at every time step. Fast Fourier Transform (FFT) is applied for determining the dimensionless vortex shedding frequency, Strouhal number St. The code computes the velocity and pressure fields, and time histories of lift, drag and base pressure coefficients, and velocity at a fixed point.

For this study of flow around both the stationary cylinders and the orbiting cylinder, the nondimensional time step was 0·0005 and the number of grid points for the majority of runs was 301 × 177, but at the lowest three Re numbers we used 201 × 118, 251 × 148, and 270 × 159, respectively, for convergence reasons. Even for the highest Re investigated, the solution was mesh independent. The computational domain shown in Fig. 1 is characterised by $R_2/R_1 = 40$. For further details see Baranyi and Shirakashi[13].

2.2 Overview of the present vortex cloud CFD method

The fundamental basis of vortex element representation of the Navier-Stokes equations has been given by the second author[6]. According to this method the entire flow is controlled by vorticity continuously being created at the body surface, diffused by viscosity and convected. The numerical method is Lagrangian in character and involves discretisation of the surface vorticity into discrete free-vortex elements which are released from the body surface at successive small time steps and subjected to convection and viscous diffusion, the latter being undertaken by random walks as defined by Chorin[20] and Porthouse[21,22].

Central to the vorticity creation process is the boundary integral equation for potential flow past an arbitrary body in the presence of a uniform stream W_∞ and a surrounding cloud of vortex elements $\Delta\Gamma_j$.

$$\begin{aligned} &\tfrac{1}{2}\gamma(s_m) + \oint k(s_m,s_n)\gamma(s_n)\mathrm{d}s_n + \mathrm{W}_\infty(\mathrm{Cos}\alpha_\infty\mathrm{Cos}\beta_m + \mathrm{Sin}\alpha_\infty\mathrm{Sin}\beta_m) \\ &+\sum_{j=1}^{Z}\Delta\Gamma_j(U_{mj}\mathrm{Cos}\beta_m + V_{mj}\mathrm{Sin}\beta_m) = 0 \end{aligned} \qquad \ldots (8)$$

The slip flow at the body surface is created by the vorticity sheet $\gamma(s)$ where, for the boundary condition of zero internal velocity inside the body, the surface velocity v_{sn} is equal to the local surface vorticity $\gamma(s_n)$.

$$v_{sn} = \gamma(s_n) \qquad \ldots (9)$$

In a viscous fluid the surface vorticity $\gamma(s)$ is being continuously created in the boundary sub-layer and diffused away from the surface where it is also subject to convective processes. For practical computations Equation (8) may be expressed in the following equivalent numerical form

$$\begin{aligned} &\sum_{1}^{M}K(s_m,s_n)\gamma(s_n) = -U_\infty\mathrm{Cos}\beta_m - V_\infty\mathrm{Sin}\beta_m \\ &-\sum_{j=1}^{Z}\Delta\Gamma_j(U_{mj}\mathrm{Cos}\beta_m + V_{mj}\mathrm{Sin}\beta_m) \end{aligned} \qquad \ldots (10)$$

where, as illustrated in Fig. 2, the body surface is represented by M elements.

Over a sequence of small time steps Δt vortex cloud theory assumes that these vortex sheets are shed as discrete vortex elements of strength $\Delta\Gamma_n = \gamma(s_n)\Delta s_n$. As indicated in Fig. 2, greater resolution may be achieved by shedding this vorticity from n_{sub} sub-elements, where, for the example of three illustrated, the discrete vortex strengths would be $\Delta\Gamma_n = \gamma(s_n)\Delta s_n/3$. In addition to this vorticity creation and shedding process for each time step Δt and in accordance with the Navier-Stokes equations, the vortex cloud is subject to convection and diffusion, the latter being accomplished by imposing random walks.

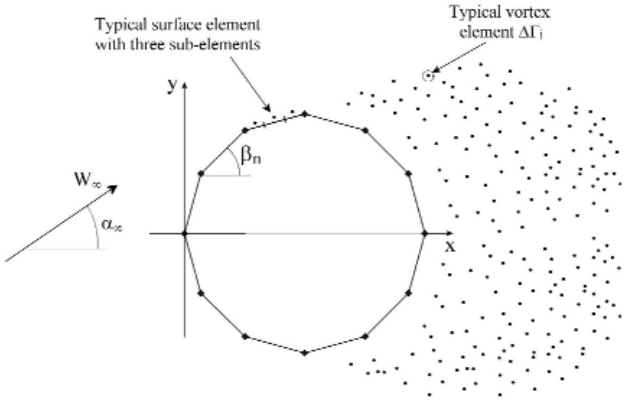

Figure 2. Numerical model for vortex cloud analysis.

2.2.1 Lift and drag forces

Lift and drag forces comprise two components due to surface pressure and shear stresses. As shown elsewhere[6] the pressure distribution on the cylinder surface at any instant may be calculated from the equation

$$\Delta p_n = -\rho \frac{\gamma(s_n)\Delta s_n}{\Delta t} = -\rho \frac{n_{sub}\Delta\Gamma_n}{\Delta t} \qquad \ldots (11)$$

where Δp_n is the pressure change along the surface of element Δs_n during the time step Δt. Pressure forces P_x and P_y on the cylinder in the x and y directions then follow from

$$P_x = \sum_{n=1}^{M} \Delta p_n \mathrm{Sin}(\beta_n), \qquad P_y = -\sum_{n=1}^{M} \Delta p_n \mathrm{Cos}(\beta_n) \qquad \ldots (12)$$

Frictional shear stresses may be estimated for each surface element by considering the shear stress after time t on a plane wall parallel to the x axis shedding surface vorticity $\gamma(s_n) = U$ at time $t = 0$. The governing equation for this, with kinematic viscosity ν and vorticity ω, is as follows,

$$\frac{\partial \omega}{\partial t} = \nu \frac{\partial^2 \omega}{\partial y^2} \qquad \ldots (13)$$

As shown by Batchelor[23], the solution is given by

$$\omega(y,t) = \frac{U}{\sqrt{\pi \nu t}} e^{-y^2/4\nu t} = \frac{\gamma(s_n)}{\sqrt{\pi \nu t}} e^{-y^2/4\nu t} \qquad \ldots (14)$$

The shear stress τ on element n over time step Δt may then be estimated from that at the wall, $y = 0$, resulting in

$$\tau = \mu \frac{du}{dy} = \mu\, \omega(y,t) = \frac{\mu\, \gamma(s_n)}{\sqrt{\pi \nu \Delta t}} \qquad \ldots (15)$$

Applying this to all surface elements, the frictional forces F_x and F_y on the cylinder then follow from

$$F_x = \rho \sqrt{\frac{\nu}{\pi \Delta t}} \sum_{n=1}^{M} \gamma(s_n)\Delta s_n \mathrm{Cos}(\beta_n), \qquad F_y = \rho \sqrt{\frac{\nu}{\pi \Delta t}} \sum_{n=1}^{M} \gamma(s_n)\Delta s_n \mathrm{Sin}(\beta_n) \qquad \ldots (16)$$

The lift and drag forces then follow from

$$L = -(P_x + F_x)\mathrm{Sin}\alpha_\infty + (P_y + F_y)\mathrm{Cos}\alpha_\infty, \qquad D = (P_x + F_x)\mathrm{Cos}\alpha_\infty + (P_y + F_y)\mathrm{Sin}\alpha_\infty \qquad \ldots (17)$$

One problem of vortex cloud analysis is the presence of significant numerical noise due to the use of random walks for simulation of viscous diffusion. Smoothing can be achieved by using a running average of say three time steps before and after the current one when evaluating lift and drag, the practice adopted here.

3.0 COMPARISON OF DETAILED C_L/C_D, STROUHAL NUMBER AND WAKE FLOW PATTERN VERSUS REYNOLDS NUMBER

As we shall see, over the chosen range of Reynolds number Re there are considerable variations of both lift coefficient C_L and drag coefficient C_D where, for a cylinder of diameter d in a uniform stream U with kinematic viscosity ν, these parameters are defined as follows:

$$\mathrm{Re} = \frac{Ud}{\nu} \qquad \ldots (18)$$

$$C_L = \frac{L}{\tfrac{1}{2}\rho U^2 d}, \qquad C_D = \frac{D}{\tfrac{1}{2}\rho U^2 d} \qquad \ldots (19)$$

Vortex street development is associated with large oscillations of C_L as Re increases above a value of about 40. A summary of the variations in amplitude of C_D and Strouhal number St predicted by the two analyses is given in Section 3.1, where, for a vortex shedding frequency f_v, St is defined as

$$St = \frac{f_v d}{U} \qquad \ldots (20)$$

The drag on a circular cylinder originates from two sources, namely pressure forces normal to the body surface or 'form drag', and viscous shear stresses parallel to the surface or 'skin friction drag' C_{Df}. For this low Re range there are also considerable variations of these and comparisons of the predicted values are given in Section 3.2. As a consequence of this the fluid motion is dominated by viscous effects at the low values Re in this range and by convective effects at high Re. This has considerable influence over the wake flow patterns and will be illustrated in Section 3.3.

3.1 Comparison of lift and drag coefficients and of Strouhal number *versus* Reynolds number

In this section comparisons are given of predicted lift coefficient and Strouhal number for the two methods of CFD analysis. To begin with in Fig. 3, comparisons are given of the predicted lift and drag coefficients for a sample mid-range value of Re = 120, assuming a uniform stream $U = 1$, a cylinder diameter of unity and an overall elapse of dimensionless time $t = 400$ well sufficient to establish the periodic motion. As may be seen from Fig 3, the lift coefficient settles down quickly into oscillating von Kármán vortex shedding with a mean value of zero. The predicted Strouhal number for the Re is of value 0·173 from the vortex cloud analysis and 0·175 from the grid-based method which compare well. As is well known, the frequency of the drag coefficient signal is double that of the lift coefficient as predicted by both methods. On the other hand there are considerable differences in the predicted time-history curves obtained by the two methods.

The grid-based analysis predicts that the motion settles down into a very regular periodic motion in which both C_L and C_D oscillate with constant amplitudes. The vortex cloud method on the other hand, exhibits some randomness in these amplitudes, although the mean values are in reasonable agreement as can be seen from the dashed

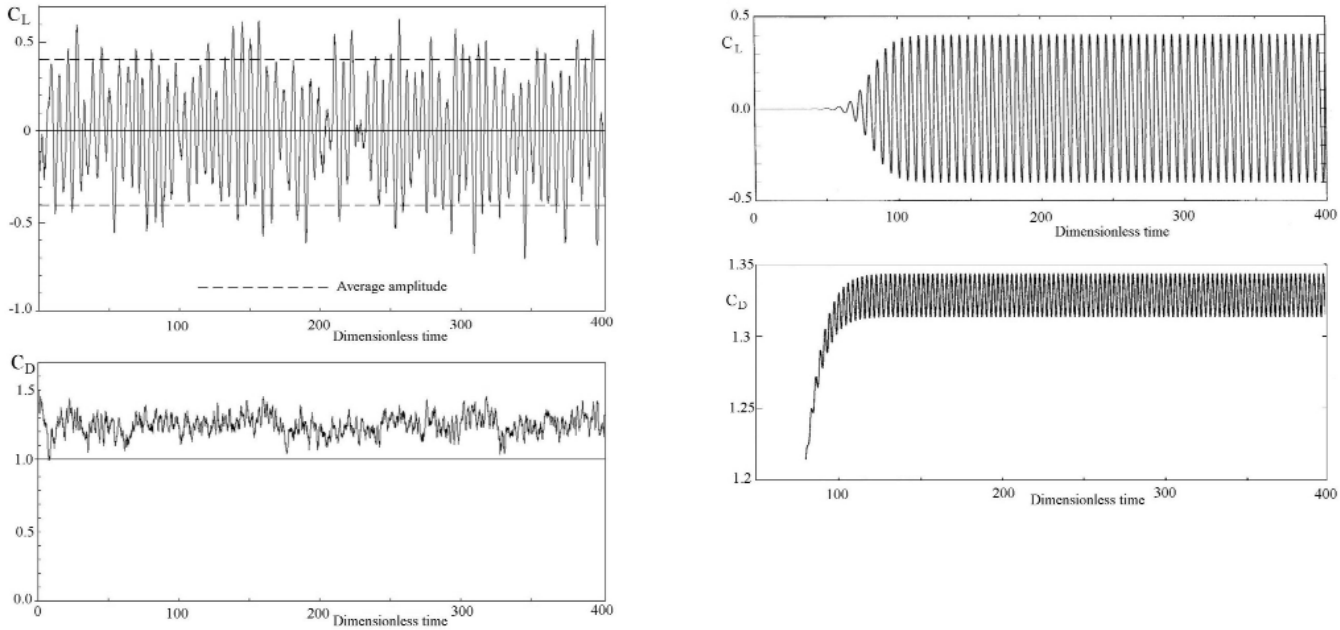

(a) Vortex cloud method

(b) Grid-based method

Figure 3. Time histories of lift and drag coefficients for Re = 120, comparison for the vortex cloud and grid-based methods.

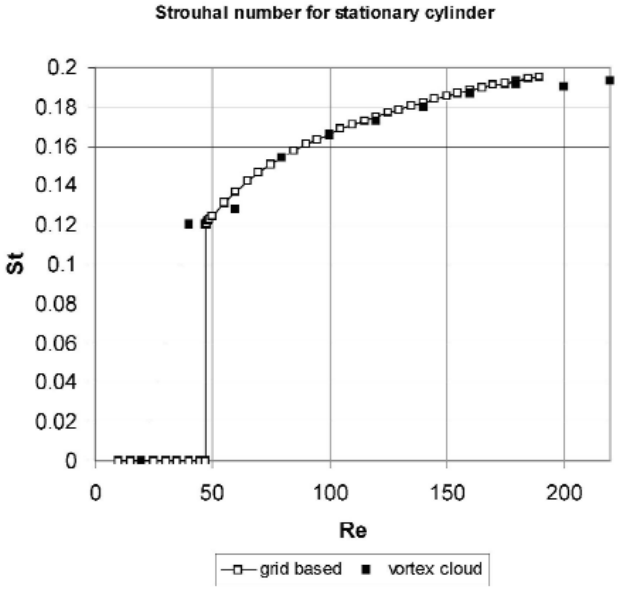

Figure 4. Comparison of the predicted Strouhal numbers.

curves in Fig. 3(a). The predicted variations of amplitude of C_L and C_D are probably due to the random walk method for simulation of viscous diffusion in vortex dynamics. However, good agreement between the methods was obtained for the two performance parameters that most affect the excitation characteristics of cylinder wake flows, the Strouhal number St and the root-mean-square value of the lift coefficient fluctuations C_{Lrms}. As further evidence of this, comparisons of the predicted values of St, C_{Drms} and C_{Lrms} versus Re for the two computational methods are given below in Figs. 4 and 5.

Figure 4 shows excellent agreement between the two methods of analysis for the predicted value of Strouhal number up to Re = 190. The grid-based analysis illustrated clearly that the onset of a von Kármán type vortex wake occurs at Re ≈ 47, below which the influence of viscous diffusion predominates over that of vortex convection (bearing in mind that vortex street formation is fundamentally a convective process). Vortex cloud simulations are in general agreement with this although it was just about possible to detect slight wake fluctuation from seven diameters downstream of the cylinder for Re = 40 and an intermittent fluctuation of C_L . Above Re = 47 however, the Strouhal number rises steadily from 0·12 to about 0·2 for Re = 210, the two numerical methods being in very good agreement. However, note that grid method computations were carried out from Re = 10 to only 190. This is because of experimental evidence from Williamson[24] and Floquet stability analysis by Barkley and Henderson[25] proving that a three-dimensional instability (mode A) begins to appear at around Re = 190. Above this Reynolds number the application of a three-dimensional code is needed to capture the three-dimensional instabilities.

The first author investigated the critical Reynolds number for the onset of vortex shedding. However, grid method computations in the vicinity of this critical Re require a very long CPU time to reach the quasi-steady state of vortex shedding (although the possibility exists that introducing turbulence into the free stream may reduce the time needed for the establishment of vortex shedding). That is why in this study the case belonging to Re = 47·2 was the nearest Reynolds number investigated above the critical one. By extrapolating the present C_{Lrms} values to zero the critical Reynolds number is about $Re_c \approx 46{\cdot}8$. Other studies have found similar values. For sufficiently large aspect ratios Norberg[26] found experimentally that the critical value of Reynolds number where periodic vortex shedding starts is about Re = 47. By extrapolating the computed values of the amplitude of oscillations of the lift coefficient Lange *et al*[27] found that the critical Reynolds number for the onset of vortex shedding is 45·9. By using the Stuart-Landau model Thompson and Le Gal[28]

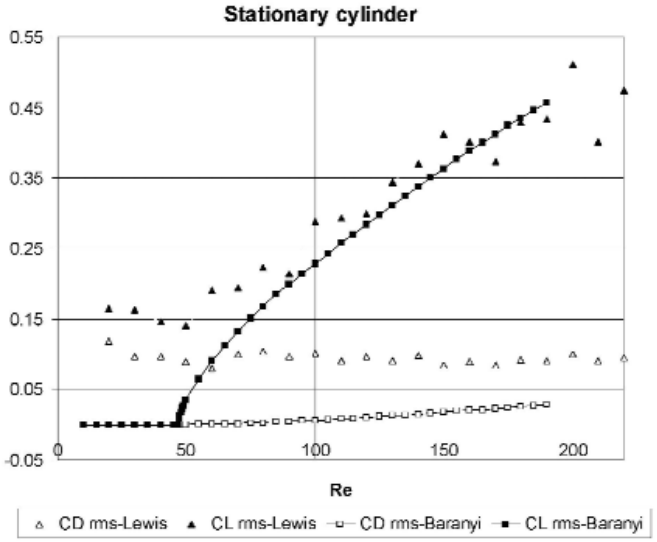

Figure 5. Variation of rms lift and drag coefficient fluctuations with Reynolds number.

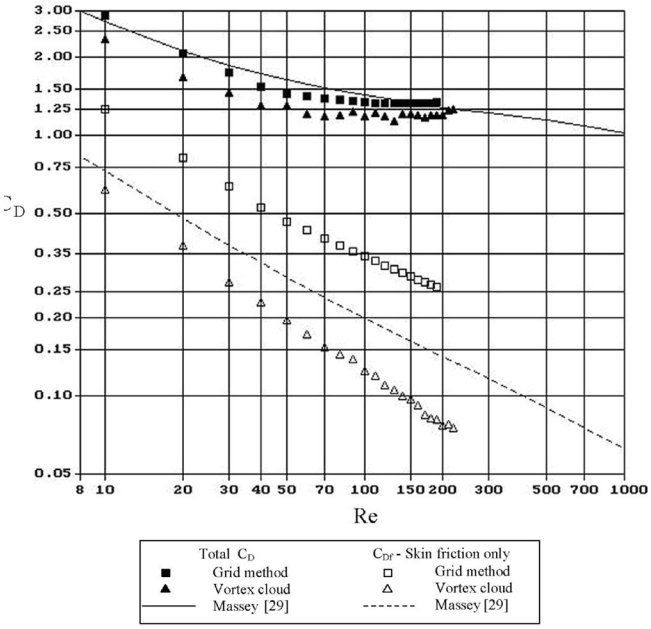

Figure 6. Comparison of predicted total and skin friction drag coefficients with published experimental values.

found that the supercritical Hopf bifurcation characterising the onset of periodic vortex shedding is at Re = 46·4.

Figure 5 shows the variation of the *rms* values of lift and drag coefficient over the chosen Re range, comparing the two CFD methods. It can easily be seen from this figure that predicted C_{Lrms} values are much larger than C_{Drms} values above the critical Reynolds number of Re ≈ 47, especially for the grid-based method. There is a good measure of agreement in C_{Lrms} between the two CFD methods in the supercritical region, albeit with a scatter in the vortex cloud results. On the other hand the predicted C_{Drms} values are excessively high for the vortex cloud method.

Below the critical value of Re ≈ 47, for which there is no von Kármán vortex street formed, it is natural that all rms values should become zero. This condition is certainly predicted by the grid method, but there are significant values of both C_{Lrms} and C_{Drms} predicted by vortex cloud analysis. The reason for this is undoubtedly due to the level of numerical discretisation in the vortex cloud method for which the time step was set at Δt = 0·05, with d = 1·0, U = 1·0. In particular the random walk simulation, which can be shown to approach molecular diffusion in the limit, is equivalent to the presence of random turbulence in the mainstream flow at this level of time step discretisation on the global scale. The effect is particularly felt at the body surface where the vortex cloud simulation of the boundary layer is at its weakest without enormous reduction of the time step, which is not a practical possibility within the current computing power available· The dramatically smaller time steps of Δt = 0·0005 used in the grid-based CFD method thus set the equivalent 'numerical turbulence' to negligible proportions and the effect of this can be seen in Fig. 3 above. Thus even with Re = 120 the vortex street oscillation takes a substantial amount of time t ≈ 70 to initiate, whereas with the vortex cloud prediction the vortex street triggers almost immediately. Once started however the dominance of the convective processes takes over and the vortex cloud method then comes into its own as shown by the predictions of Strouhal number, Fig. 4.

Detailed predicted values delivered by the grid method are recorded in the Appendix for the dimensionless frequency of vortex shedding i.e. Strouhal number (St), time-mean and rms values of lift, drag, drag due to skin friction, and base pressure coefficients for Re = 100-190.

3.2 Comparison of predicted form and skin friction drag components

The final comparison of the two CFD methods is shown in Fig. 6, namely predicted values of both the total drag coefficient C_D and the skin friction component of this C_{Df} compared also with experimental results published by Massey[29] for the selected Re range. As Massey's[29] results in the figure show, the total drag coefficient falls very considerably over the range 10 < Re < 200 from about 2·75 to 1·25 (a ratio of 2·2) and both methods predict this trend well, the grid method particularly so. It is encouraging to see this mutual agreement over such an important widely varying Re range of twenty to one, within which the shift transfers from the dominance of viscous effects to those of convective processes (as will be illustrated by other considerations in Section 3.0 and Table 1 below). Thus also from Massey's data the skin friction drag component falls from roughly C_{Df} = 0·75 to 0·14 over this Re range (a ratio of 5·4!) and is thus only a small fraction of the total drag but decreasing to negligible values at the top end of the Re range. The two CFD methods here produce predictions that lie on either side of Massey's experimental results, reflecting the general dramatic trends while not in such good agreement.

3.3 Illustration of predicted flow patterns (vortex cloud method) for low Reynolds numbers

One advantage of the vortex cloud method is the economy in modelling wake patterns by the cloud of discrete vortices, which can then also be viewed in movie style. Application of this method for the selected Re range resulted in the comparisons presented in Fig. 7 which reveal the developing significant changes in wake pattern. These were undertaken with a long elapse of time allowing a mainstream traverse of no less than one hundred cylinder diameters.

As may be seen from these predictions, the onset of periodic vortex shedding only begins to appear above Re = 20, below which viscous diffusion is sufficiently dominant over convection to avert this. At the higher Reynolds number of 60 however a very regular

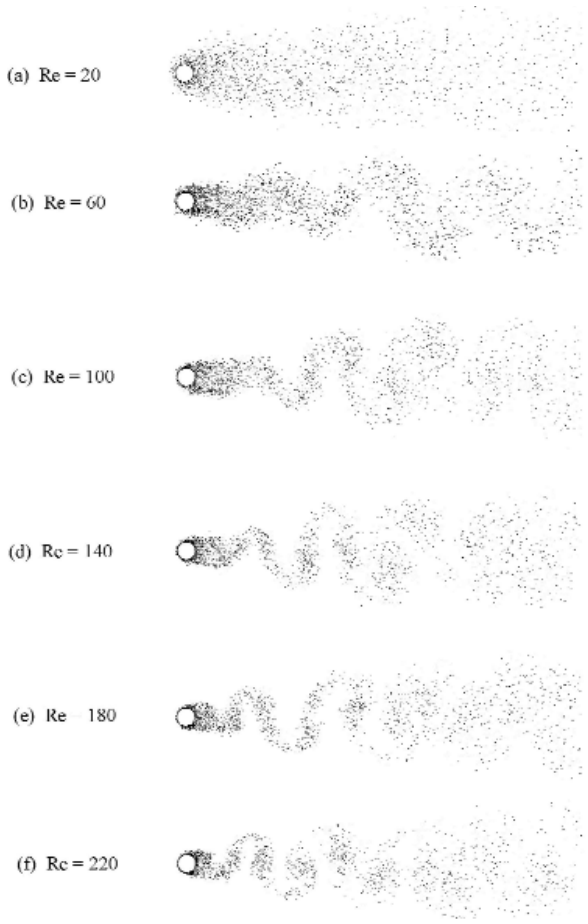

Figure 7. Predicted vortex shedding flow patterns for Re range 20 to 220.

wake periodicity is established which continues right through the higher Re range up to Re = 220. Through Re = 100-140 the actual vorticity wake sheet thins down to a fairly constant thickness in the near wake oscillations. At the higher Re range of 180-220 however, one observes that as convection begins to dominate over diffusion, the near wake oscillations begin to roll up into distinct vortex cores while remaining still in a regular vortex street pattern.

A simple analysis that bears up this expectation follows from a comparison of the average convective and diffusive displacements of a typical vortex element as a function of Reynolds number. Assuming an average convective velocity of say ½U, the average convective displacement Δx_{av} of a vortex cloud element during a time step Δ_t would thus be $\Delta x_{av} = ½U\Delta t$. As also shown by Lewis[6], the radial shift of a typical vortex element during the viscous diffusion random walk may be expressed through

$$\Delta r_i = \sqrt{4\nu\Delta t \ln(1/P_i)} \quad \ldots (21)$$

where P_i is a random number in the range 0-1·0. The average random walk shift Δr_{av} for $P_i = 0{\cdot}5$ is thus

$$\Delta r_{av} = \sqrt{4\nu\Delta t \ln 2} \;=\; 2\sqrt{(Ud\Delta t \ln 2)/\mathrm{Re}} \quad \ldots (22)$$

Table 1 compares the predicted average convective and diffusive shifts Δx_{av} and Δr_{av} for $10 \le \mathrm{Re} \le 300$. The extremely interesting

Table 1
Comparison of typical average element convective and diffusive displacements during one time step in the vortex cloud analysis for U = 1·0, d = 1·0, Δt = 0·05

Re	Average convective shift Δr_{av}	Average diffusive shift Δr_{av}
10	0·025	0·117741
20	0·025	0·083255
60	0·025	0·048068
100	0·025	0·037230
140	0·025	0·031468
180	0·025	0·027752
220	**0·025**	**0·025101**
260	0·025	0·023091
300	0·025	0·021496

observation to be made here is that Δx_{av} and Δr_{av} for a typical vortex element are equal when $\mathrm{Re} \approx 220$. Thus convective processes may be expected to dominate above this Re value and diffusive processes below it, in agreement with the vortex wake motions presented in Fig. 7. At the lowest value of Re = 10 tabulated here however, the average diffusive shift of the vortex cloud random walk process is almost five times the average convective shift of the vortex elements. It should be mentioned that for this Reynolds number the numerical vortex cloud scheme arranges for the random walk simulation of viscous diffusion to be undertaken in five sub-steps to maintain equal resolution with the convective process.

4.0 CONCLUSIONS

Two completely different computational fluid dynamic simulation techniques based on a grid and on vortex dynamics have been compared for the classic datum case of flow past a stationary circular cylinder over the low Reynolds number range $10 \le \mathrm{Re} \le 220$ with the following conclusions:

1. Both methods are in good agreement in prediction of the Strouhal number which varies between $0{\cdot}12 < St < 0{\cdot}2$ over the Re range considered, and both predict the establishment of a von Kármán type vortex street above $\mathrm{Re} \approx 47$. Furthermore, using the grid method and extrapolating the C_{Lrms} values to zero, the critical Reynolds number belonging to the onset of vortex shedding was found to be about $\mathrm{Re}_c \approx 46{\cdot}8$.

2. Both methods are in reasonable agreement with the experimental measurements published by Massey[29] and with one another for the total drag coefficient C_D. Predictions of the contribution to this due to skin friction C_{Df} are in less good agreement but show similar trends.

3. Predictions of the *rms* fluctuations in lift and drag, C_{Lrms} and C_{Drms} are in less good agreement. The grid CFD method predicts zero values of these below the critical level Re = 47 due to the complete absence of a vortex street and rapidly rising values $0{\cdot}0 < C_{Lrms} < 0{\cdot}46$ for $47 < \mathrm{Re} < 190$. Vortex cloud results agree with the latter reasonably well but predict excessive values of both C_{Lrms} and C_{Drms} for subcritical Reynolds numbers Re < 47.

4. With regard to the last mentioned item, it is pointed out that the grid CFD calculations used extremely small time steps Δt = 0·0005 resulting in tight control of the discretisation errors in this time sensitive motion. The vortex cloud method on the other hand here used time steps 100 times bigger, namely Δt = 0·05 resulting in one hundred times the scale of equivalent 'numerical turbulence'. The main impact of this is of course felt within the

body boundary layer due to the use of the random walk method for simulation of viscous diffusion and thus the consequent surface vorticity creation over each time.

5. It was found that the predicted average convective and diffusive shifts of a typical vortex element during a time step become equal at about Re = 220. Above this, convective processes become more dominant.

6. Vortex dynamics handles the overall vortex street motions, heavily dominated by convective processes, extremely well providing also easy graphical presentation of the vortex street wake patterns. Furthermore the method has proved extremely flexible for adaptation to any other stationary or moving body and has been useful for simulating such other phenomena as rotating stall in turbomachinery blade rows.

ACKNOWLEDGEMENT

The support provided by the Hungarian Research Foundation (OTKA, project No T 042961) is gratefully acknowledged by the first author. We also thank Mr S. Ujvárosi for preparing Fig. 6.

REFERENCES

1. STROUHAL, V. Über eine besondere Art der Tonerregung, *Ann Phys und Chemie Nav Series*, 1878, **5**, pp 216-251.
2. KARMAN T. von Über ein Mechanismus des Widerstandes, den ein bewegter Körper in einer Flüssigkeit erfährt, *Göttingen Nachrichten Maths, -Phys*, 1911, KI, pp 509-517.
3. ROSENHEAD, L. The formation of vortices from a surface of discontinuity, *Proc Roy Soc A*, 1931, **134**, pp 170-192.
4. ABERNATHY, F.H. and KRONAUER, R.E. The formation of vortex streets, *J Fluid Mech*, 1962, **13**, pp 1-20.
5. BARANYI, L. Numerical simulation of flow past a cylinder in orbital motion, *J Comp App Mech*, 2004, **5**, (2), pp 209-222.
6. LEWIS, R.I. *Vortex Element Methods for Fluid Dynamic Analysis of Engineering Systems*, 1991, Cambridge University Press, Cambridge.
7. ROSHKO, A. On the development of turbulent wakes from vortex streets, *NACA Rep*, 1954, **1191**.
8. NORBERG, C. Flow around a circular cylinder: aspects of fluctuating lift, *J Fluid Struct*, 2001, **15**, pp 459-469.
9. BEARMAN, P.W. Developments in the understanding of bluff body flows, *Proc JSME Centennial Grand Congress*, 1997, **1**, pp 53-61, Int Conf on Fluid Eng, Tokyo.
10. KAWAMURA, T. and KUWAHARA, K. Computation of high Reynolds number flow around a circular cylinder with surface roughness, *AIAA-84-0340*, 1984, pp 1-11, Proc 22nd Aerospace Sciences Meeting 1984, Reno, Nevada.
11. BRAZA, M., CHASSAING, P. and MINH, H.H. Numerical study and physical analysis of the pressure and velocity fields in the near wake of a circular cylinder, *J Fluid Mech*, 1986, **165**, pp 79-130.
12. KARNIADAKIS, G.E. and TRIANTAFYLLOU, D.S. Frequency selection and asymptotic states in laminar wakes, *J Fluid Mech*, 1989, **199**, pp 441-469.
13. BARANYI, L. and SHIRAKASHI, M. Numerical solution for laminar unsteady flow about fixed and oscillating cylinders, *Comp Assisted Mech. and Eng Sci*, 1999, **6**, pp 263-277.
14. BARANYI, L. Computation of unsteady momentum and heat transfer from a fixed circular cylinder in laminar flow, *J Comp App Mech*, 2003, **4**, (1), pp 13-25.
15. ROSHKO, A. Perspectives on bluff body aerodynamics, *J Wind Eng Ind Aerod*, 1993, **49**, pp 79-100.
16. BARANYI, L. and LAKATOS, K. Computational fluid dynamics analysis of low Reynolds number flow around stationary and oscillating cylinders, Proc Fourth Int Eng Conf, Mansoura-Sharm El-Shiekh, 2004, **1**, pp 459-465.
17. NORBERG, C. Fluctuating lift on a circular cylinder: review and new measurements, *J Fluid Struct*, 2003, **17**, pp 57-96.
18. DE SAMPAIO, P.A.B. A finite element formulation for transient incompressible viscous flows stabilized by local time-steps, *Comput Methods Appl Mech Engrg*, 2005, **194**, pp 2095-2108.
19. FLETCHER, C.A.J. *Computational Techniques for Fluid Dynamics*, 1997, Vol 2, Second Ed, Springer, Berlin.
20. CHORIN, A.J. Numerical study of slightly viscous flow, *J Fluid Mech*, 1973, **57**, pp 785-796.
21. PORTHOUSE, D.T.C. Numerical Simulation of Aerofoil and Bluff Body Flows by Vortex Dynamics, 1983, PhD thesis, University of Newcastle upon Tyne.
22. PORTHOUSE, D.T.C. and LEWIS, R.I. Simulation of viscous diffusion for extension of the surface vorticity method to boundary layer and separated flows, *J Mech Eng Sci*, 1981, **23**, (3), pp 157-167, I Mech E.
23. BATCHELOR, G.K. *An Introduction to Fluid Dynamics*, 1970, Cambridge UP, Cambridge.
24. WILLIAMSON, C.H.K. Vortex dynamics in the cylinder wake, *Annu Rev Fluid Mech*, 1996, **28**, pp 477-539.
25. BARKLEY, D. and HENDERSON, R.D. Three-dimensional Floquet stability analysis of the wake of a circular cylinder, *J Fluid Mech*, 1996, **322**, pp 215-241.
26. NORBERG, C. An experimental investigation of the flow around a circular cylinder: influence of aspect ratio, *J Fluid Mech*, 1994, **258**, pp 287-326.
27. LANGE, C.F., DURST, F. and BREUER, M. Momentum and heat transfer from cylinders in laminar crossflow at $10^{-4} \leq Re \leq 200$, *Int J Heat Mass Tran*, 1998, **41**, pp 3409-3430.
28. THOMPSON, M.C. and LE GAL, P. The Stuart-Landau model applied to wake transition revisited, *Eur J Mech B-Fluid*, 2004, **23**, pp 219-228.
29. MASSEY, B.S. *Mechanics of Fluids*, 1989, Sixth Ed, Van Nostrand Reinhold, London.

APPENDIX

Predicted values of the dimensionless frequency of vortex shedding i.e. Strouhal number (*St*), time-mean and rms values of lift, drag, drag due to skin friction and base pressure coefficients for Re = 10 - 190 delivered by the grid method are recorded on the opposite page.

Re	C_{Lrms}	C_{Dmean}	C_{Drms}	C_{Dfmean}	$C_{Df\,rms}$	$\lvert C_{pbmean}\rvert$	C_{pbrms}	St
10	0	2·8776	0	1·2602	0	0·7192	0	0
15	0	2·3620	0	0·9814	0	0·6231	0	0
20	0	2·0630	0	0·8212	0	0·5759	0	0
25	0	1·8761	0	0·7145	0	0·5478	0	0
30	0	1·7360	0	0·6371	0	0·5282	0	0
35	0	1·6284	0	0·5778	0	0·5136	0	0
40	0	1·5425	0	0·5305	0	0·5017	0	0
45	0	1·4718	0	0·4918	0	0·4917	0	0
47	0	1·4468	0	0·4782	0	0·4879	0	0
47·2	0·0079	1·4467	0·00003	0·4775	0	0·4903	0·00070	0·1197
47·3	0·0097	1·4467	0·00003	0·4772	0	0·4914	0·00067	0·1201
47·5	0·0127	1·4464	0·00003	0·4765	0	0·4934	0·00064	0·1204
48	0·0185	1·4454	0·00004	0·4746	0	0·4980	0·00063	0·1214
48·5	0·0232	1·4441	0·00005	0·4727	0·00001	0·5021	0·00064	0·1222
49	0·0274	1·4427	0·00007	0·4707	0·00001	0·5059	0·00064	0·1230
50	0·0349	1·4395	0·00010	0·4668	0·00001	0·5129	0·00068	0·1246
55	0·0651	1·4225	0·00033	0·4480	0·00004	0·5423	0·00120	0·1312
60	0·0903	1·4071	0·00067	0·4311	0·00009	0·5674	0·00216	0·1369
65	0·1127	1·3939	0·00112	0·4160	0·00014	0·5903	0·00342	0·1422
70	0·1330	1·3825	0·00166	0·4025	0·00020	0·6113	0·00492	0·1464
75	0·1514	1·3726	0·00230	0·3902	0·00027	0·6309	0·00668	0·1505
80	0·1684	1·3640	0·00301	0·3791	0·00034	0·6493	0·00861	0·1543
85	0·1844	1·3566	0·00379	0·3689	0·00042	0·6667	0·01073	0·1575
90	0·19971	1·3501	0·00462	0·3596	0·00050	0·6833	0·01290	0·1608
95	0·2145	1·3446	0·00549	0·351	0·00059	0·6992	0·01521	0·1635
100	0·2289	1·3400	0·00642	0·3431	0·00068	0·7147	0·01763	0·1661
105	0·2430	1·3361	0·00740	0·3358	0·00077	0·7298	0·02074	0·1688
110	0·2570	1·3329	0·00842	0·3289	0·00086	0·7445	0·02283	0·1708
115	0·2708	1·3304	0·00950	0·3226	0·00095	0·7600	0·02566	0·1730
120	0·2845	1·3284	0·01061	0·3167	0·00105	0·7733	0·02863	0·1751
125	0·2980	1·3269	0·01177	0·3111	0·00115	0·7874	0·03171	0·1769
130	0·3114	1·3258	0·01295	0·3059	0·00124	0·8013	0·03492	0·1788
135	0·3247	1·3252	0·01416	0·3010	0·00134	0·815	0·03816	0·1806
140	0·3378	1·3249	0·01539	0·2964	0·00143	0·8286	0·04149	0·1821
145	0·3508	1·3249	0·01664	0·2920	0·00153	0·8421	0·04487	0·1838
150	0·3636	1·3252	0·01791	0·2879	0·00163	0·8554	0·04830	0·1853
155	0·3761	1·3258	0·01920	0·2840	0·00172	0·8686	0·05182	0·1867
160	0·3885	1·3266	0·02050	0·2802	0·00181	0·8817	0·05538	0·1882
165	0·4006	1·3275	0·02181	0·2767	0·00191	0·8945	0·05898	0·1895
170	0·4125	1·3286	0·02314	0·2733	0·00200	0·9073	0·06263	0·1908
175	0·4242	1·3299	0·02447	0·2700	0·00209	0·9198	0·06633	0·1919
180	0·4356	1·3312	0·02581	0·2669	0·00218	0·9322	0·07008	0·1930
185	0·4468	1·3327	0·02715	0·2639	0·00227	0·9445	0·07388	0·1942
190	0·4577	1·3342	0·02849	0·2611	0·00235	0·9565	0·07770	0·1953